

Adsorptive Removal of Iron and Manganese from Groundwater Samples in Ghana by Zeolite Y Synthesized from Bauxite and Kaolin

Item Type	Journal article
Authors	Williams, Craig;Kwaky-Awuah, Bright;Sefa-Ntiri, Baah;Von-Kiti, Elizabeth;Nkrumah, Isaac
Citation	Kwaky-Awuah, B., Sefa-Ntiri, B., Von-Kiti, E. and Williams, C. (2019) Adsorptive Removal of Iron and Manganese from Groundwater Samples in Ghana by Zeolite Y Synthesized from Bauxite and Kaolin, Water, 11(9), 1912; https://doi.org/10.3390/w11091912
DOI	10.3390/w11091912
Publisher	MDPI
Journal	Water
Download date	2026-04-17 02:37:36
License	https://creativecommons.org/licenses/by/4.0/
Link to Item	http://hdl.handle.net/2436/622539

Article

Adsorptive Removal of Iron and Manganese from Groundwater Samples in Ghana by Zeolite Y Synthesized from Bauxite and Kaolin

Bright Kwakye-Awuah ^{1,*}, Baah Sefa-Ntiri ², Elizabeth Von-Kiti ³, Isaac Nkrumah ¹ and Craig Williams ⁴

¹ Department of Physics, Kwame Nkrumah University of Science and Technology, UPO, PMB, Kumasi, Ghana; inkrumah.sci@knust.edu.gh

² Department of Physics, University of Cape Coast, UPO, PMB, Cape Coast, Ghana; bsefa-ntiri@ucc.edu.gh

³ Council for Scientific and Industrial Research—Institute of Industrial Research, P.O. BOX LG 576 Accra, Ghana; evonkiti@csir-iir.com

⁴ Faculty of Science and Engineering, University of Wolverhampton, Wolverhampton WV1 1LY, UK; c.williams@wlv.ac.uk

* Correspondence: bkwakye-awuah.cos@knust.edu.gh; Tel.: +233-545-207159

Received: 13 May 2019; Accepted: 15 June 2019; Published: 13 September 2019



Abstract: Ground water samples from residential homes in three Regions of Ghana: Central, Greater Accra and Ashanti, were analyzed for iron and manganese contamination. The samples were exposed to characterized zeolite Y by X-ray diffraction, scanning electron microscopy, energy dispersive X-ray spectroscopy, Fourier transformed-infrared spectroscopy and thermogravimetric-differential thermal analysis. Zeolite Y is able to remove 98% of iron and 97% of manganese within an hour. The adsorption of both iron and manganese followed the Freundlich model, suggesting that the ions were transported onto the zeolite Y surface and subsequently diffused into the zeolite Y framework. The kinetic studies showed that pseudo-first order and intra particle and film diffusion models provided the best fit. The adsorption at $0.2 \text{ mg L}^{-1} \text{ Fe}$ ($Q_{0.2}$) is calculated to be 0.023 mg g^{-1} for the Freundlich adsorption model, whilst that of manganese at $0.05 \text{ mg L}^{-1} \text{ Mn}$ ($Q_{0.05}$) is evaluated to be 0.015 mg g^{-1} . The zeolite retains its adsorption properties when retrieved from the first exposure water sample, washed copiously with distilled water and added to fresh water samples. The results suggest that zeolite Y can be used as a potential adsorbent for the removal of iron and manganese from groundwater.

Keywords: bauxite; kaolin; zeolite Y; iron; manganese; removal efficiency; adsorption

1. Introduction

Iron and manganese occur in dissolved forms as single ions (Fe^{2+} , Mn^{2+}) or in undissolved higher forms mainly as Fe(II) or Mn(II), respectively [1]. Both metals are common elements found in the earth's crust [2], and are two of the most common pollutants found in both surface and groundwater, but predominantly in the latter [3,4], reaching the ground water by the rain, surface and waste water filtration dissolving minerals from soil strata. The Fe(II) and Mn(II) ions pollution in groundwater may interact with the sediment and with other dissolved constituents, such as inorganic anions, or dissolved organic carbon (DOC), present as a humic-like material [4]. These interactions lead to complex formations and to potential solid precipitation. Iron may also be present as a result of the use of the iron coagulants of the corrosion of steel and cast iron pipes during ground water extraction and distribution [5,6]. Both elements can be commonly found in natural water in concentrations up to 1.0 mg L^{-1} , although they are rarely present in concentrations exceeding 1.0 mg L^{-1} [3,4].

The presence of iron in water causes aesthetic and operational problems such as odor and a brown color, stain and deposition in the water distribution systems, leading to high turbidity [5–7]. Colored water is formed when oxidized iron enters the bulk water as ferric particles or as Fe(II) and forms ferric particles [6,8]. Manganese is also used in the manufacture of iron and steel alloys, manganese alloys and as an ingredient in various products [9]. Elevated levels of manganese in water is considered undesirable, because when water is exposed to air, Mn(II) is oxidized to Mn(IV). This Mn(IV) precipitate can stain household utensils and clothes, and may impart a metallic, bitter, astringent or medical taste to water [3]. Exposure to high concentrations of manganese over the course of years has been associated with a nervous system disease with symptoms like Parkinson's disease [10].

Several techniques and methods are employed in the removal of manganese and iron from water, including aeration, settling, filtration and ion exchange [11–13]. The use of low-cost materials as potential sorbents for the removal of heavy metals has been emphasized recently, and among the different materials which possess sorbent properties are zeolites [12,13]. Natural and synthetic zeolites are used as a filtration material for the removal of iron and manganese from water [12]. Zeolites are microporous aluminosilicates minerals which could be used as ion exchange in domestic and commercial water purification, softening and other applications [14,15]. Substitution of silicon by aluminum atoms in the crystal framework leads to an extra negative charge to be balanced by the surrounding counter ions (such as Na^+ , K^+ , Ca^{2+} , and Mg^{2+}), and these counter ions are easily exchanged by the cations of a contact solution with better affinity [15,16]. A number of earlier studies confirm their excellent performance in the removal of heavy metals from underground water [1,6,17–19]. Although there are many papers on the utilization of natural zeolites, the synthetic zeolites can also be used for the same purpose because the synthetic zeolites resemble the natural zeolite minerals [17]. Natural zeolites are cheaper compared to synthetic zeolites, but contain other impurities such as quartz, iron, copper, lead and rare earth metals. These supposed impurities make natural zeolites less effective compared to synthetic zeolites. Synthetic zeolites, however, are expensive, but are also very effective, since they can be synthesized for a specific application and purpose.

Zeolite Y is considered one of the most promising candidates for use in the removal of metal ions from water, owing to their large pore high surface structure [20–22]. Synthetic zeolites are produced from chemical reagents. However, in this work there is an added benefit to the environment and human health, since the synthetic zeolite Y produced for this study was obtained by transforming bauxite and kaolin. The synthesis protocol developed by our research group is novel, and is currently being documented for a possible patent right. Earlier studies by Shevade [23] and Ford showed that modified zeolite Y with NH_4^+ can remove arsenic from water and Yusof and coworkers [18] also reported that synthesized zeolite NaY from rice husks can remove chromate and arsenate ions from aqueous solutions. The aims of this paper are to synthesize zeolite Y from bauxite and kaolin in Ghana, and to investigate its capability to remove iron and manganese from natural ground water samples.

2. Materials and Methods

2.1. Materials and Reagents

Natural raw materials: Bauxite and kaolin were sampled from the Ghana Bauxite Mining Company site, at Awaso in the Western Region of Ghana. Sodium hydroxide (Analar grade) was purchased from Analar Normapur, UK, and distilled water was obtained from the Water Research laboratory, KNUST. Bauxite was sampled from Awaso in the Western Region particularly close to the Ghana Bauxite Company site. The kaolin and bauxite were ground and sieved with a $0.75\ \mu\text{m}$ mesh sieve under dry conditions.

2.2. Method

2.2.1. Synthesis of Zeolite Y

20 g of the powdered bauxite was digested in a 200 mL sodium hydroxide solution at 2 M concentration. The slurry was stirred until it was homogenized and heated at 130 °C for 5 h in an electrical oven, after which the solution was filtered off the red mud, and stored in polypropylene containers. In addition, 40 g of sodium hydroxide was dry-mixed with 30 g of kaolin and calcined at 600 °C for 2 h to obtain sodium metakaolinite, after which the mixture was allowed to cool to room temperature, and then added to 500 mL of distilled water. The mixture was stirred for 30 min until a homogeneous slurry was obtained. A 100 mL portion of the bauxite filtrate was added to the slurry and the mixture was stirred for 1 h, whereby they were homogenized. The slurry was then transferred into 1 L Teflon® (Polytetrafluoroethylene—PTFE, Cowie Technology, Middlesbrough, UK) bottles, and heated in an electric oven for 5 h for the zeolite crystals to precipitate. At the end of the 5 h, the Teflon® bottles were removed from the oven, quenched in running tap water and cooled to room temperature, after which they were filtered off and washed copiously with distilled water. Zeolite crystals were dried overnight in an electric oven at 100 °C, crushed into fine powder and stored in zip lock plastic containers.

2.2.2. Characterization of Zeolite Y

All characterizations were carried out at the Faculty of Science and Engineering, University of Wolverhampton, United Kingdom. A PANalytical Empyrean Powder X-ray diffractometer (PANalytical, Malvern, UK) was used to collect data using Bragg-Brentano geometry and a slit configuration of a degree fixed divergence slit of 0.25°.

Using a ZEISS EVO50 scanning electron microscope equipped with Energy Dispersive X-ray analyzer (EDX), the morphology of the starting materials and the as-synthesized zeolites, as well as their chemical compositions, were determined by a Zeiss EVO 500 (Zeiss, Cambridge, UK). Bauxite, kaolin and zeolite powder samples were dry sprayed onto aluminum stubs using double-sided adhesive carbon discs. They were then coated with gold to decrease static charging during their observation under SEM conditions.

The vibrational properties as well as the chemical bonds present in the samples were analyzed with a Mattson Fourier transformed-infrared (FT-IR) spectrometer (Mattson Instruments, Milton Keynes, UK) equipped with the ZnSe crystal plate attached to the spectrometer with a mercury cadmium telluride. The (MCTA) detector and KBr as a beam splitter was used to analyze the samples. Measurements were done using 100 scans at 4 cm⁻¹ resolution, units of log (1/R) (absorbance), over the mid-IR region of 1200–400 cm⁻¹.

2.2.3. Groundwater Sampling

All samples were collected using the clean sampling procedures specified by the Ghana Standard Authority. Water samples were collected from boreholes directly from the ground before entering the main pipe. Physicochemical characteristics such pH, turbidity, and conductivity were measured at the well site with a Hydrolab H₂O connected in-line through a flow through cell. Before a ground-water sample was collected for laboratory analysis, wells were purged for a period of at least 20 min until the above field characteristics had stabilized. Stability was determined on the basis of the following criteria: A specific conductance variation less than 2 µS/cm, a pH variation less than 0.05 pH units, a dissolved oxygen variation less than 0.05 mg L⁻¹, and a temperature variation of less than 1 °C. Alkalinity titrations were performed on filtered samples in the field. All wells were sampled for an analysis of major cations, major anions, nutrients, and arsenic. A complete list of laboratory analyses is included in Table 1. The samples were acidified with 0.1 M HNO₃ to a pH of 6.5 (slightly acidic), and stored in refrigerator in a dark room to prevent any partial oxidation of the iron and manganese in the water. Hence, fairly constant initial concentrations were maintained throughout the period of the analysis.

2.2.4. Continuous Retrieval and Re-Use of Zeolite Y

The extent to which zeolite Y persisted in its adsorption activity was investigated according to the method given by Kwakye-Awuah et al. [24,25] with some modifications. Starting with the water samples from Cape Coast, 3 g of zeolite Y was added to 300 mL of sample in conical flasks and shaken on an orbital shaker for 120 min after which the zeolite was filtered, washed copiously with distilled water and air-dried in a fume cupboard and finally oven dried at 50 °C in an electric oven for 3 h. 2.0 g of the retrieved zeolite was added to 200 mL of the fresh water sample and the procedure was repeated. In the third successive reuse of the zeolite, 1.0 g of the zeolite was added to 100 mL of fresh water in order to maintain constant zeolite, and water volume ratio, and adsorption activity was investigated as before. The entire procedure was repeated for water samples from Ashesi and Kumasi.

2.2.5. Chemical Analysis and Batch Adsorption Experiment

The manganese and iron concentrations were determined using Atomic Absorption Spectrophotometer (AAS) (Perkin Elmer, Beaconsfield, UK) and results were expressed as mgFeL⁻¹ or mgMnL⁻¹. The solution pH was determined using a pH meter (Hannah Instruments, Buzzard, UK). Batch ion-exchange experiments were carried out in seven 250 mL conical flasks. Starting with the Cape Coast sample, 100 mL portion of water sample were placed in each conical flask and 1.0, 2.0, 2.5, 3.0, 3.0, 4.0 and 4.5 g of zeolite Y added. The flasks were then placed on an orbital shaker at 25 °C, at a constant agitation of 50 rpm. Supernatant was collected and filtered through a Whatman filter paper number 1 before chemical analysis to remove zeolite particles that may be present in the supernatant. The pH was measured for each sampling time thrice, and the average pH was evaluated.

2.2.6. Kinetic Studies

The kinetic studies of Fe and Mn onto zeolite Y were conducted using the same procedure during 120 min. However, aliquot samples were taken at 0, 10, 20, 30, 40, 60, 90 and 120 min respectively. Supernatant aliquots were filtered through an 8 mL filter before chemical analysis. The pH was measured for each sampling time thrice, and the average pH was then evaluated.

2.3. Theoretical Model Equations

The adsorption Q_e of Fe and Mn by zeolite Y was evaluated by the use of Equation (1).

$$Q_e = \left(\frac{C_o - C_e}{m} \right) V \quad (1)$$

where C_o is the initial iron or manganese concentration (mg Fe²⁺ L⁻¹ or mg Mn²⁺ L⁻¹), C_e is the final concentration (mg Fe L⁻¹ or mg Mn L⁻¹), V is the batch volume (L) and m is the adsorbent mass (g). Having characterized water samples from all three locations and confirmed identical drinking water parameters, the adsorption studies were performed on samples from Ashesi only, since the mechanism of adsorption of the samples from the Cape Coast and Kumasi were not likely to be different from that of Ashesi.

Determination of the adsorption capacity at various equilibrium concentrations C_e (time contact long enough) was performed by obtaining the experimental adsorption isotherm, commonly described by the Langmuir and/or Freundlich models. These models are given, respectively, by Equations (2) and (3):

$$Q_e = \frac{Q_{max} K_L C_e}{1 + K_L C_e} \quad (2)$$

$$Q_e = K_F C_e^{\frac{1}{n}} \quad (3)$$

The linearized form of Equations (2) and (3) are given as:

$$\frac{C_e}{Q_e} = \frac{1}{K_L Q_{max}} + \frac{C_e}{Q_{max}} \quad (4)$$

$$\log Q_e = \log K_F + \frac{1}{n} \log C_e \quad (5)$$

where the Langmuir parameters given by Q_{max} ($\text{mg Fe}^{2+} \text{ g}^{-1}$ or $\text{mg Mn}^{2+} \text{ g}^{-1}$) and K_L ($\text{L mg}^{-1} \text{ Fe}^{2+}$ or $\text{L mg}^{-1} \text{ Mn}^{2+}$) are the maximum capacity adsorption at high equilibrium concentrations and the equilibrium constant. The Freundlich parameters K_F ($\text{mg g}^{-1} (\text{Lmg}^{-1})^{\frac{1}{n}} \text{ Fe}^{2+}$ or $\text{mg g}^{-1} (\text{Lmg}^{-1})^{\frac{1}{n}} \text{ Mn}^{2+}$) and $1/n$ are the Freundlich capacity factor and the Freundlich intensity parameter, respectively.

The kinetics of the Fe and Mn adsorption were evaluated by applying four different models: (1) The pseudo-first-order kinetic model; (2) pseudo-second-order kinetic model; (3) intra-particle diffusion model and; (4) the liquid film diffusion model. The Lagergren pseudo-first-order kinetic model for the adsorption of a liquid/solid system is based on solid uptake capacity. This model assumes that the rate of uptake with time is directly proportional to the difference in the saturation concentration and the amount (cumulative) of solute uptake with time. The general equation is expressed as [26]:

$$\frac{dQ_t}{dt} = K_1(Q_e - Q_t) \quad (6)$$

where Q_e and Q_t are the amounts of metal ions (Fe^{2+} or Mn^{2+}) adsorbed (mg g^{-1}) at equilibrium and at time t , respectively, and K_1 is the Lagergren pseudo-first order adsorption rate constant (min^{-1}). Integrating Equation (6) for the boundary condition $t = 0$ to $t = t$ and $Q = 0$ to $Q = Q_t$, the linear form of the equation becomes:

$$\log(Q_e - Q_t) = \log(Q_e) - \frac{K_1 t}{2.303} \quad (7)$$

The pseudo-second-order kinetic model is based on the amount of adsorbate on the adsorbent. If the rate of adsorption is a second order mechanism, the pseudo-second-order chemisorption kinetics rate equation is expressed as:

$$\frac{dQ_t}{dt} = K_2(Q_e - Q_t)^2 \quad (8)$$

where K_2 is the second-order adsorption rate constant ($\text{g mg}^{-1} \text{ min}^{-1}$). Integrating Equation (8) between the same limits, the linear form of the equation is given by [26]:

$$\frac{t}{Q_t} = \frac{1}{K_2 Q_e^2} + \frac{1}{Q_e} t \quad (9)$$

Metal ions are transported from aqueous phase to the surface of the adsorbent and subsequently they can diffuse into the interior of the particles if they are porous. The intra-particle diffusion is governed by Equation (6), where K_i is the intra-particle diffusion rate constant ($\text{g mg}^{-1} \text{ min}^{1/2}$):

$$Q_t = K_i t^{\frac{1}{2}} \quad (10)$$

In a situation where the transport of the adsorbate from the liquid phase up to the solid phase boundary plays the most significant role in adsorption, the liquid film diffusion model, Equation (11), may be applied [27]:

$$\ln(1 - F) = -K_{fd} t \quad (11)$$

where F is the fractional attainment of equilibrium ($F = Q_t/Q_e$) and K_{fd} is the adsorption rate constant which is dependent on the adsorbent. A linear plot of $\ln(1 - F)$ versus t with zero intercept would suggest that the kinetics of the adsorption process is controlled by diffusion through the liquid film surrounding the solid adsorbent.

3. Results

3.1. Characterization of Zeolite Y

The diffractogram of the zeolite Y sample is shown in Figure 1. Rietveld analysis conducted on the sample showed that the dominant phases were sodium zeolite Y and hydrosodalite. Hydrosodalite is a dense super cage structure that transformed to a zeolite phase upon further crystallization. Simplified spectrum is shown in the inset.

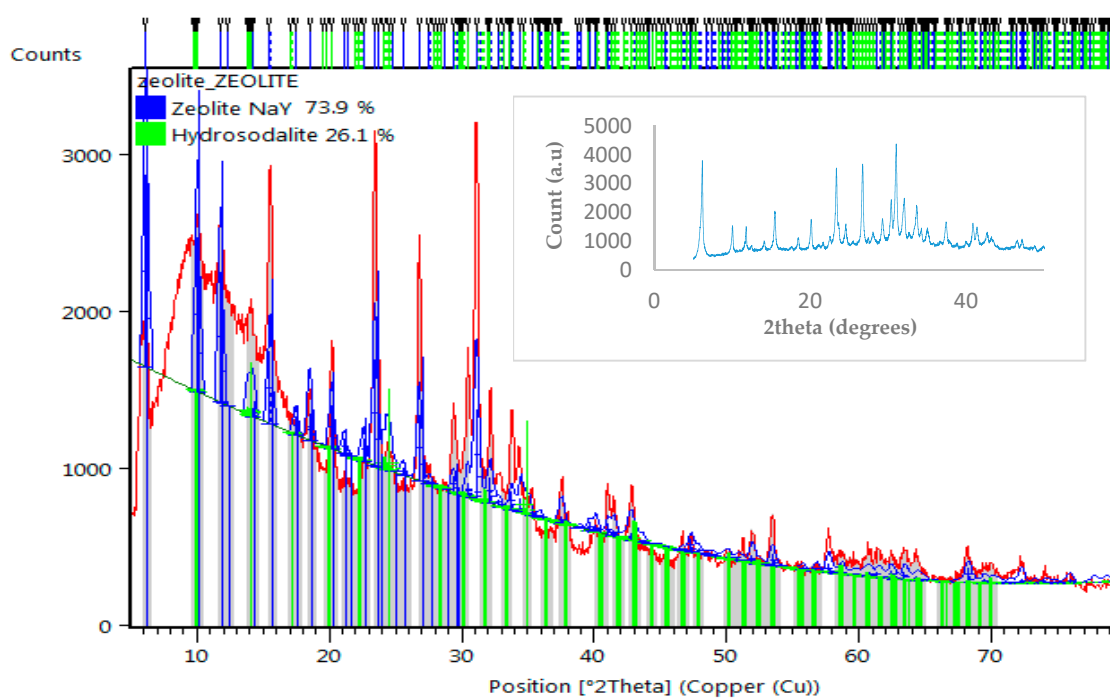


Figure 1. Experimental X-ray diffraction spectrum obtained for zeolite Y. Rietveld analysis confirms 74% zeolite Y phase and 26% hydrosodalite zeolite phase, as shown. The data from the simplified version of the experimental spectrum were plotted and presented as a simplified spectrum, as shown in the inset.

The scanning electron micrograph obtained is shown in Figure 2. The morphology of the crystals were mostly cubic, confirming that zeolite Y was the main phase.

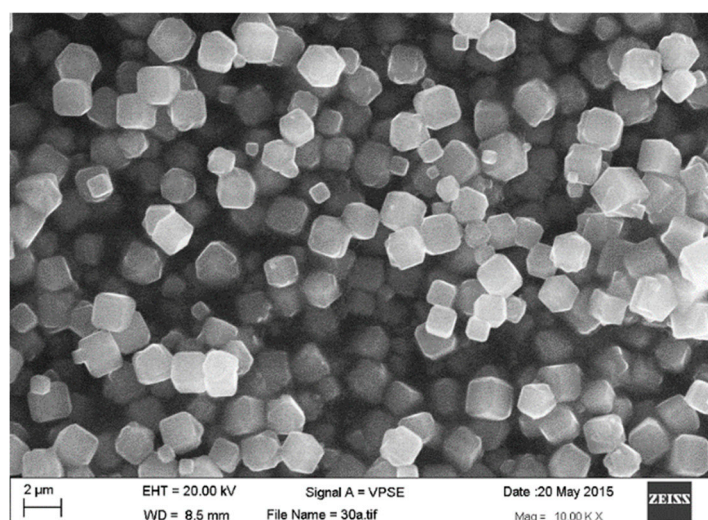


Figure 2. Scanning electron micrograph obtained for the synthesized zeolite Y.

This study showed that zeolite Y contained a complement of exchangeable sodium, potassium, and calcium ions. The zeolite contained a high percentage of Si, followed by Al, and Na as shown in Figure 3.

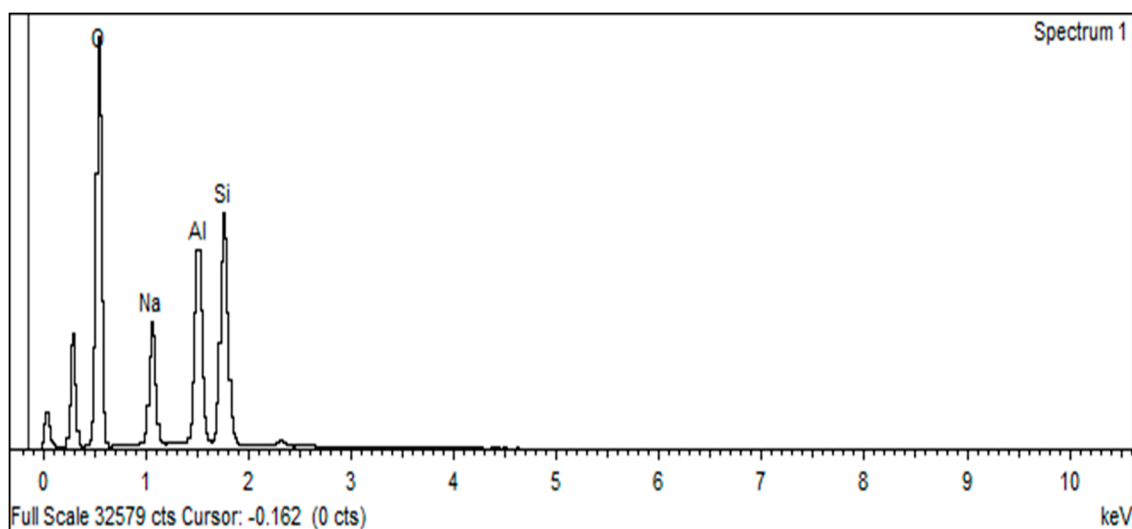


Figure 3. Energy dispersive X-ray spectrum obtained for zeolite Y. The first two un-named peaks represent carbon and gold, as the samples were gold-coated prior to the analysis. The corresponding atomic concentrations are presented in Table 1 below.

Table 1. Elemental composition of zeolite Y.

Element	% Atomic
Na	5.13
Al	35.04
Si	58.09
K	1.03
Ca	0.67
LoI	0.04
Total	100

The bands occurred at wavenumbers well within that of synthesized zeolite Y produced from chemical reagents as given by our previous works [25,26] and Mozgawa [27].

The Fourier transformed infrared spectrum obtained is presented in Figure 4. The position of the peaks formed depicts clearly that the dominant phase was zeolite Y. Bands were formed at the following wave numbers: 1624 cm, 947 cm (very strong), 743 cm (weak shoulder), 665 cm and 557 cm (moderate) and 444 cm (strong). According to Mozgawa [27] and Kwakye-Awuah et al. [28], the very strong band formed at 947 cm is attributed to the overlap of the asymmetric vibrations of the Si–O (bridging) and Si–O– (non-bridging) bonds. The symmetric stretching due to the internal vibrations of the zeolite Y framework tetrahedra occurred at 665 cm with a weak shoulder at 743 cm, whilst vibrations associated with the double six rings (D6R) that connect the sodalite cages occurred at 557 cm. The band at 444 cm is assigned to the internal vibrations due to the bending of the T–O tetrahedral [27–29]. Thermogravimetric analysis of zeolite Y (Figure 5) showed that weight losses were most apparent at 200 °C and 500 °C. The losses at 200 °C are most attributed to an evaporation of water molecules within the zeolite framework, whilst those losses at 500 °C are mostly attributed to the escape of CO₂ or the evaporation of water molecules within the hydrosodalite cavity.

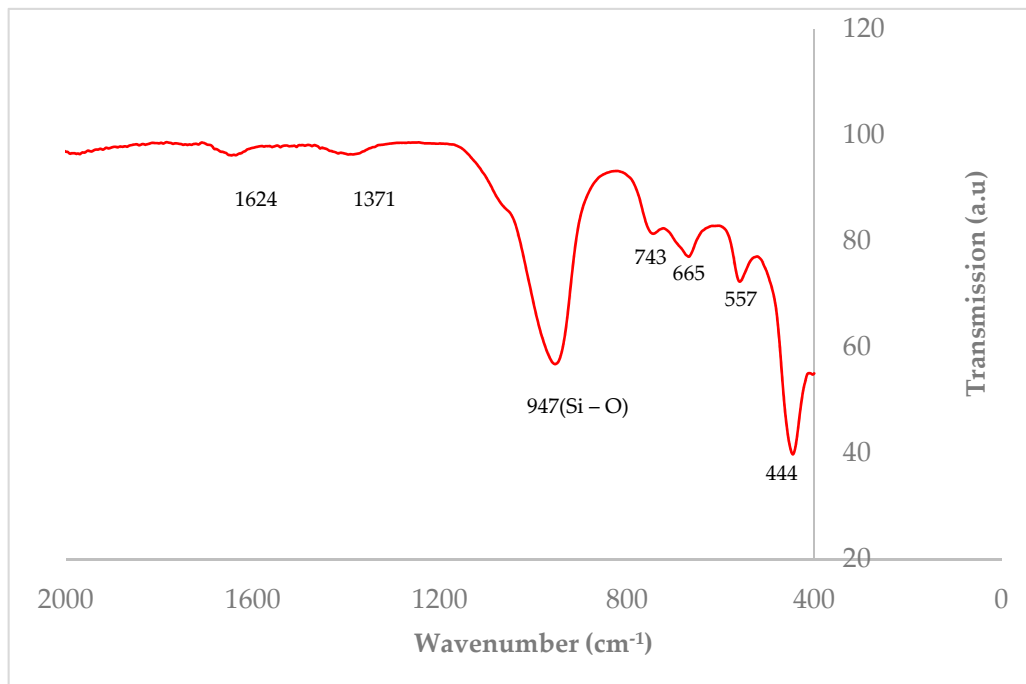


Figure 4. Spectrum obtained for Fourier-transformed infrared spectrometry (FT-IR) analysis of synthesized zeolite Y sample.

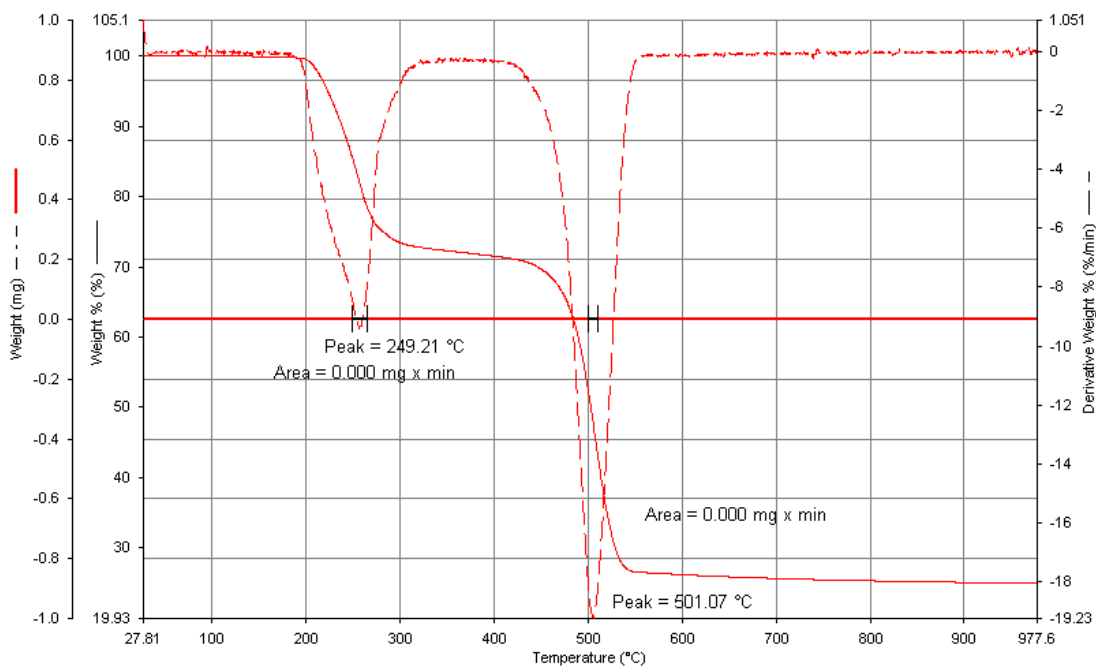


Figure 5. Thermogravimetric/Differential thermal spectrum of zeolite Y. The zeolite was heated from 30–800 °C at a heating rate of 5 °C/min.

3.2. Characterization of Water Samples

Each sample was first characterized according to Standards, approved by the World Health Organization (WHO) and adopted by the Ghana Standard Authority. The standard values of drinking water parameters given by the Ghana Standard Authority. A summary of the characterized raw water samples collected from Cape Coast, Ashesi and Kumasi are presented in Table 2.

Table 2. Characterized raw water samples from Cape Coast, Ashesi and Kumasi after treatment with zeolite Y.

Parameter	Units	Cape Coast		Ashesi		Kumasi		GSA * Standard	WHO Standard
		Before	After	Before	After	Before	After		
pH @ 25 °C		6.60	7.17	6.50	7.33	6.88	7.35	6.5–8.5	6.5–8.5
Turbidity	NTU	2.6	1.2	2.2	1.3	2.4	1.3	5 or less	50 or less
Total dissolved solids	NTU	288	280	286	278	290	282	1000	300 or less
Apparent Color	-	19	15	20	16	19	15	-	1000
Conductivity	$\mu\text{S cm}^{-1}$	500	370	570	375	590	375	2500	2500
Total hardness	mg L^{-1}	118	40	50	39	50	39	500	Not included
Ca hardness	mg L^{-1}	6.49	6	6.5	6	6.8	6	50	500
Mg hardness	mg L^{-1}	25	b.d	26	b.d	25	b.d	50	50
HCO_3^-	mg L^{-1}	23	21	20	21	22	20	400	200
Chlorides as Cl ⁻	mg L^{-1}	87		89		86		250	250
Sulphate as SO_4^{2-}	mg L^{-1}	0	0	0	0	0	0	200	200
Nitrate		0	0	0	0	0	0	50	50
Nitrite	mg L^{-1}	b.d	b.d	b.d	b.d	b.d	b.d	0.3	0.5
Cyanide	mg L^{-1}	b.d	b.d	b.d	b.d	b.d	b.d	0.07	0.05
Mercury	mg L^{-1}	b.d	b.d	b.d	b.d	b.d	b.d	0.001	0.001
Lead as Pb^{2+}	mg L^{-1}	b.d	b.d	b.d	b.d	b.d	b.d	0.01	0.01
Arsenic as As^{5+}	mg L^{-1}	b.d	b.d	b.d	b.d	b.d	b.d	0.01	0.01
Cadmium as Cd^{2+}	mg L^{-1}	b.d	b.d	b.d	b.d	b.d	b.d	0.03	0.01
Manganese	mg L^{-1}	1.61	0.08	1.54	0.05	1.35	0.04	0.05	0.2
Iron	mg L^{-1}	1.15	0.06	1.12	0.05	1.01	0.04	0.3	0.3

* = Ghana Standard Authority, b.d = below detection.

The initial Fe concentrations in the water samples were 1.15, 1.12 and 1.01 mg L^{-1} for Cape Coast, Ashesi and Kumasi, respectively, whilst that of the manganese were 1.61, 1.54 and 1.35 mg L^{-1} for Cape Coast, Ashesi and Kumasi, respectively. The pH values were 6.6 ± 0.1 , 6.5 ± 0.1 and 6.88 ± 0.1 for Cape Coast, Ashesi and Kumasi, respectively. The limits set by the WHO for iron and manganese are 0.3 and 0.05 mg L^{-1} , respectively. The Ghana Standards however, are set at 0.3 and 0.2 mg L^{-1} . Thus, the target removal levels are 85% for Fe and 97% for Mn for WHO and 85% for Fe and 87.6% for the Ghana standard. All experiments were performed in batch mode at ambient conditions (25 °C). Other water parameters were below the detection limit of the AAS instrument. After exposure to zeolite Y, the pH of all samples were within the WHO and Ghana Standard acceptable range. Some physical parameters, such as conductivity, total dissolved solids, calcium and magnesium concentration were improved after exposure of samples to zeolite Y. Furthermore, iron and manganese were found to have been removed well within the WHO and Ghana Standard Authority required limits. Removal efficiencies of iron were 98.26%, 98.21% and 97.03% for water samples from Cape Coast, Ashesi and Kumasi, respectively, whereas the removal efficiencies of 97.5%, 97.40% and 97.80% were obtained for manganese at Cape Coast, Ashesi and Kumasi, respectively. When the zeolite was retrieved from the samples and added to fresh water samples, the removal efficiencies of iron were 98.28%, 97.37% and 98.18% for samples from Cape Coast, Ashesi and Kumasi, respectively, whilst for manganese the efficiency was 97.50% and 98.03% and 97.81% for Cape Coast, Ashesi and Kumasi, respectively. Finally, upon the second retrieval, removals of 98.33%, 97.37% and 98.02% were obtained for iron and 97.52%, 98.05% and 97.78% were obtained for manganese as shown in Table 3. Thus the zeolite retained its removal efficiency after three repeated reuse.

Table 3. Removal efficiency of zeolite Y on iron and manganese in underground water samples. The amount of zeolite Y used were 3 g per 300 mL water sample for first exposure, 2 g per 200 mL water sample for first retrieval, and 1 g per 100 mL water sample for the second retrieval.

Activity	Sample Source	Initial Concentration (mg L ⁻¹)		Final Concentration (mg L ⁻¹)		Removal Efficiency (%)	
		Iron	Manganese	Iron	Manganese	Iron	Manganese
First exposure	Cape Coast	1.15	1.61	0.02	0.04	98.26	97.52
	Ashesi	1.12	1.54	0.02	0.04	98.21	97.37
	Kumasi	1.01	1.35	0.03	0.03	97.03	97.78
First Retrieval	Cape Coast	1.16	1.6	0.02	0.04	98.28	97.50
	Ashesi	1.14	1.52	0.03	0.04	97.37	98.03
	Kumasi	1.10	1.37	0.02	0.03	98.18	97.81
Second retrieval	Cape coast	1.2	1.61	0.02	0.04	98.33	97.52
	Ashesi	1.14	1.54	0.03	0.03	97.37	98.05
	Kumasi	1.01	1.35	0.02	0.03	98.02	97.78

3.3. Adsorption Studies

The adsorption of zeolite Y was found to be dependent on the mass of the zeolite used. Increasing the mass of zeolite increased the adsorption of both the iron and manganese, resulting in a fairly constant decrease in the equilibrium concentration (Figure 6). Adsorption of iron and manganese increased steadily up to 60 min. Thereafter, the rate was almost negligible. This trend of removal may be attributed to the rapid utilization of readily available adsorbing sites in the zeolite resulting in the fast diffusion. The successful zeolite retrieval and reuse (Table 3), however, implies that the zeolite did not reach its saturation. Hence, equilibrium was not attained.

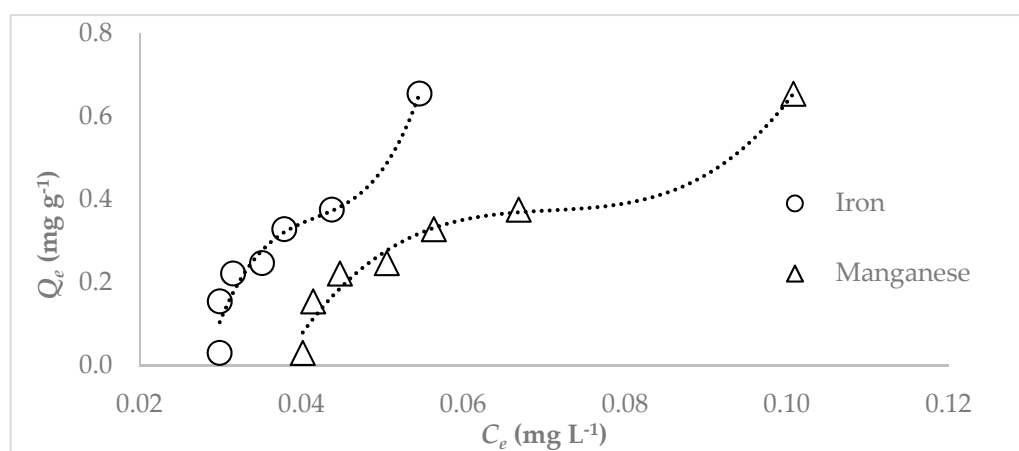


Figure 6. Graph obtained for iron and manganese uptake onto zeolite Y during adsorption studies. Initial Fe = 1.15 mg L⁻¹; Initial Mn = 1.61 mg L⁻¹; adsorbent dose = 1.0, 2.0, 2.5, 3.0, 3.0, 4.0 and 4.5 g L⁻¹, T = 25 °C; water pH = 6.5.

It can be seen from Figure 7 that adsorption of Fe(II) and Mn(II) increased with mass 1.0, 2.0, 2.5, 3.0, 3.0, 4.0 and 4.5 g L⁻¹ of zeolite Y used. The highest adsorption occurred with mass = 4.5 g per 100 mL water sample. Adsorption also increased rapidly at the initial stages up to 60 min (Figure 7) Beyond 60 min the increased in adsorption did not show a sharp increase, indicating that the zeolite was approaching equilibrium concentrations. However, the successive efficiency obtained for the three retrievals (Table 4) is attributed to the fact that the used Zeolite Y sample did not reach the adsorption capacity at the corresponding equilibrium.

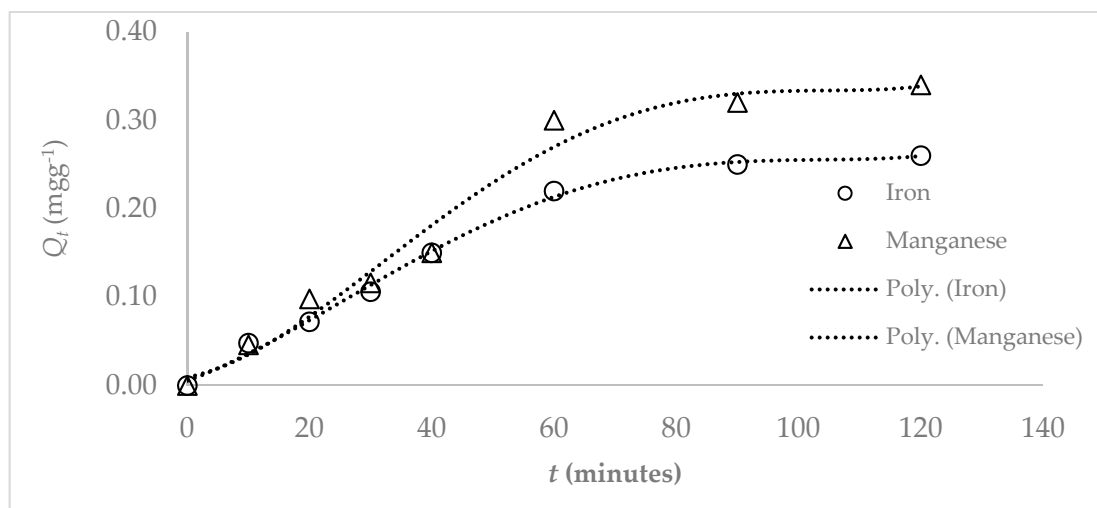


Figure 7. Graph obtained for iron and manganese uptake onto zeolite Y during adsorption studies with time. Initial Fe = 1.15 mg L⁻¹; Initial Mn = 1.61 mg L⁻¹; adsorbent dose = 2.5 g L⁻¹, T = 25 °C; water pH = 6.5.

Table 4. Adsorption isotherms parameters for iron and manganese onto zeolite Y.

	Langmuir			Freundlich		
	Q_{max} (mg g ⁻¹)	K_L (L mg ⁻¹)	R^2	K_F (mg g ⁻¹ (L mg ⁻¹) ^{1/n})	$1/n$	R^2
Fe	31.45	1.551	0.626	0.0618	0.6145	0.979
Mn	18.02	1.881	0.664	0.1216	0.6922	0.981
				$Q_{Fe=0.2} = 0.023$		
				$Q_{Mn=0.05} = 0.015$		

Adsorption isotherms for Langmuir and Freundlich models for iron and manganese are shown in Figures 8 and 9. The R^2 values derived from the Langmuir fitting was 0.626 for iron and 0.664 for manganese, whereas values of 0.979 and 0.981 were obtained from the Freundlich model for iron and manganese, respectively. The adsorption isotherm becomes favorable for $1/n < 1$ (or $n > 1$), unfavorable for $1/n > 1$ (or < 1) and linear for $n = 1$. The values of $1/n$ obtained for Fe(II) and Mn(II) were 0.0645 and 0.1246. Thus the adsorption of both Fe(II) and Mn(II) appears to follow the Freundlich model, and not the Langmuir model.

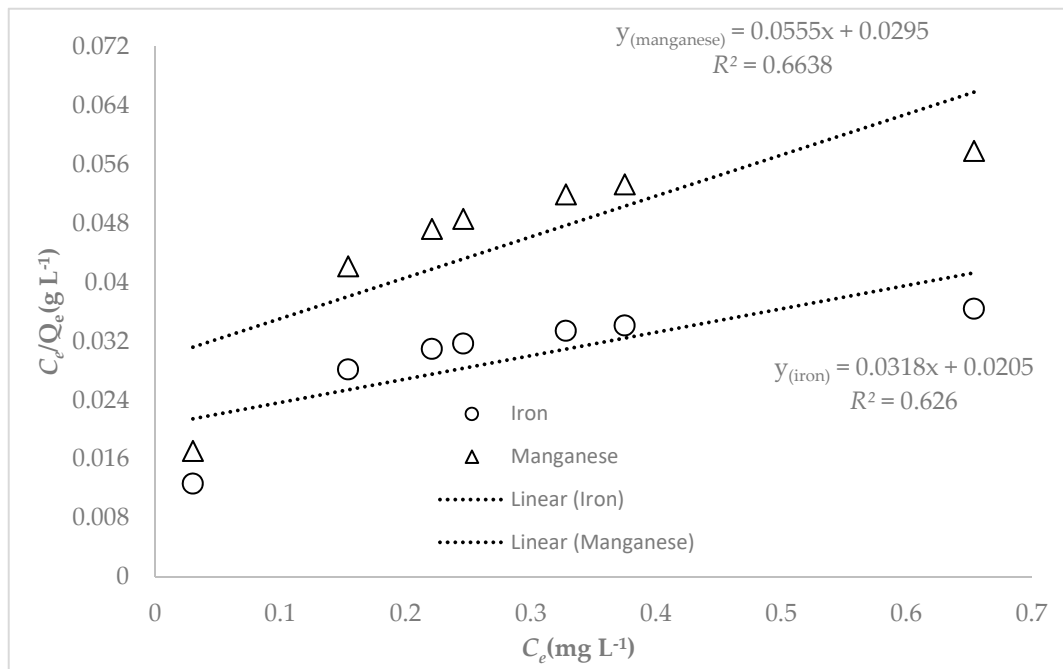


Figure 8. Non-linearized Langmuir adsorption isotherms obtained for the iron and manganese uptake onto zeolite Y during the adsorption studies. Initial Fe = 1.15 mg L⁻¹; Initial Mn = 1.61 mg L⁻¹; adsorbent dose = 1.0, 2.0, 2.5, 3.0, 3.0, 4.0 and 4.5 g L⁻¹, T = 25 °C; water pH = 6.5.

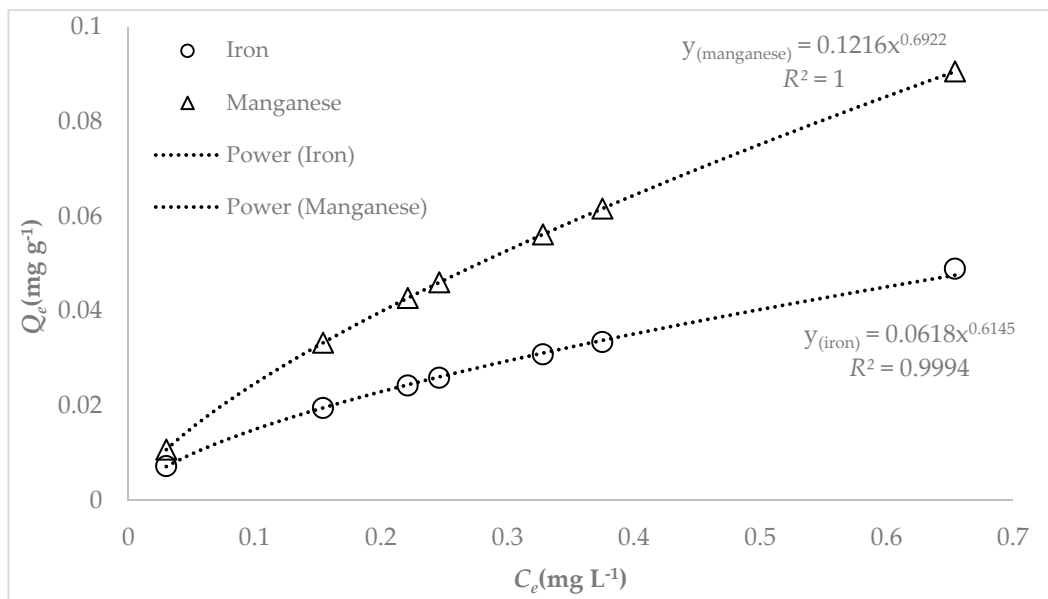


Figure 9. Non-linearized Freundlich adsorption isotherms obtained for the iron and manganese uptake onto zeolite Y during the adsorption studies. Initial Fe = 1.15 mg L⁻¹; Initial Mn = 1.61 mg L⁻¹; adsorbent dose = 1.0, 2.0, 2.5, 3.0, 3.0, 4.0 and 4.5 g L⁻¹, T = 25 °C; water pH = 6.5.

4. Discussion

The plot of adsorption capacity versus time showed that the kinetics of the Fe and Mn adsorption onto adsorbent consisted of two phases: An initial rapid adsorption phase that continued for at least 60 min, and subsequently a very slow second sorption phase, with small contributions to the total Fe and Mn adsorption uptake, while after 60 min the change of adsorption capacities for both Fe and Mn did not show a sharp increase. The first phase can be attributed to either intra-particle diffusion or mass transfer from the bulk liquid to the particle external surface, since the suspension was vigorously

agitated during the adsorption experiments. As more of Fe and Mn are adsorbed onto the zeolite sorption sites, the zeolite becomes saturated, thereby decreasing the sorption capacity. In this respect, Saha et al. [30] explained that at low metal concentrations metals are mainly sorbed onto specific sorption sites, while at higher metal concentrations the sorption sites overlap, becoming thus less specific for a particular metal. This in turn, induces a reduction in metal sorption. Consequently, less favorable sites were involved in the sorption process as Fe(II) and Mn(II) saturate the action sorption sites in the aqueous solution. The mechanism of the sorption of Fe and Mn is attributed to both the ion exchange and adsorption processes. During the ion exchange process, Fe and Mn move through the pores of the zeolite mass, but also through channels of the lattice, replacing exchangeable cations (mainly sodium, potassium and calcium).

The Langmuir parameter Q_{max} represents the monolayer saturation whilst the Freundlich parameter n indicates the binding affinity for Fe(II) and/or Mn (II). The R^2 values (0.526 for iron and 0.664 for manganese) obtained for the Langmuir model for both iron and manganese showed that the Langmuir model did not provide a good fit for the adsorption of Fe(II) and Mn(II). The Freundlich constant, K_F , (adsorption capacity) values obtained were $0.0618 \text{ mg g}^{-1} (\text{L mg}^{-1})^{\frac{1}{n}}$ for iron and $0.1216 \text{ mg g}^{-1} (\text{L mg}^{-1})^{\frac{1}{n}}$ for manganese. The corresponding $\frac{1}{n}$ values were 0.6145 for iron and 0.6922 for manganese. The $\frac{1}{n}$ values at equilibrium for both iron and manganese were less than 1, reflecting a favorable adsorption of Fe(II) and Mn(II). Furthermore, the corresponding adsorption at 0.2 mg L^{-1} Fe ($Q_{0.2}$) was calculated to be 0.023 mg g^{-1} , whilst that of manganese at 0.05 mg L^{-1} Mn ($Q_{0.05}$) was calculated to be 0.015 mg g^{-1} . The values obtained for the Freundlich parameter were found to be in agreement with what were obtained from other workers such as Fu et al. [31], Guozinis et al. [32], Farag et al. [33], Yuvuz et al. [34], Wei-Wei et al. [35] and Araby et al. [36].

From Table 5 it can also be found that the calculated $Q_e = (0.221 \text{ mg g}^{-1})$ for Fe(II) for the pseudo-first order reaction were on a par with the experimental Q_e value (0.220 mg g^{-1}) for the observed process. However, there were considerable differences for Mn(II) between the calculated value (0.250 mg g^{-1}) and the experimental (0.282 mg g^{-1}) value. Unlike the pseudo first-order equation considerable differences were observed between calculated Q_e values for Fe(II) and Mn(II) and the experimental Q_e . The values of the first and second reaction rate constants K_1 , K_2 obtained from sorption kinetic models were used to correlate the experimental data on zeolite Y. It is worthy to note that the pseudo-first reaction constant has a higher value for the sorption kinetic of iron and manganese than those obtained from pseudo-second order kinetics. Furthermore, the R^2 values obtained indicate a better correlation for pseudo-first order (Figure 10) compared with pseudo-second order (Figure 11) kinetics. Hence, these values mean that the sorption followed first-order kinetics.

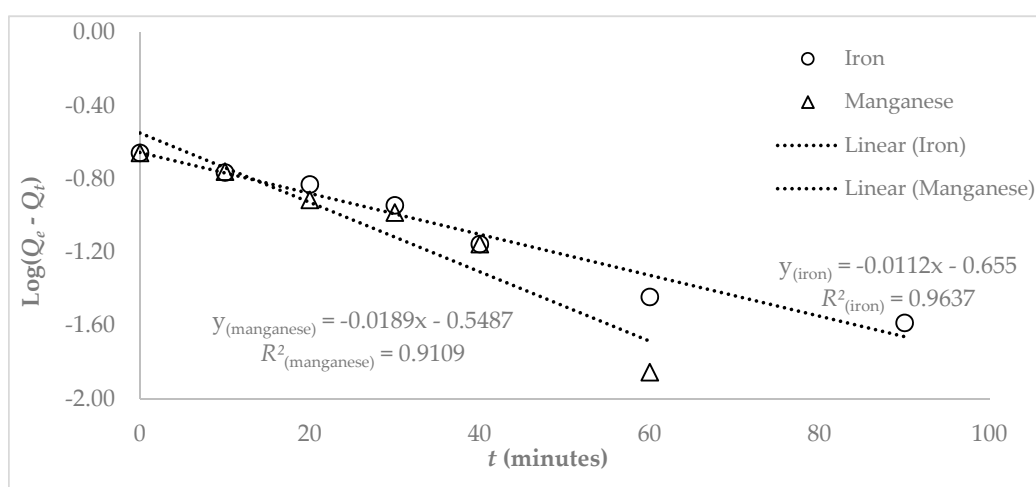


Figure 10. Pseudo first-order kinetic model obtained for adsorption of iron and manganese on to zeolite Y. Initial Fe = 1.15 mg L^{-1} ; Initial Mn = 1.61 mg L^{-1} ; adsorbent dose = 2 g L^{-1} , T = $25 \text{ }^\circ\text{C}$; water pH = 6.5.

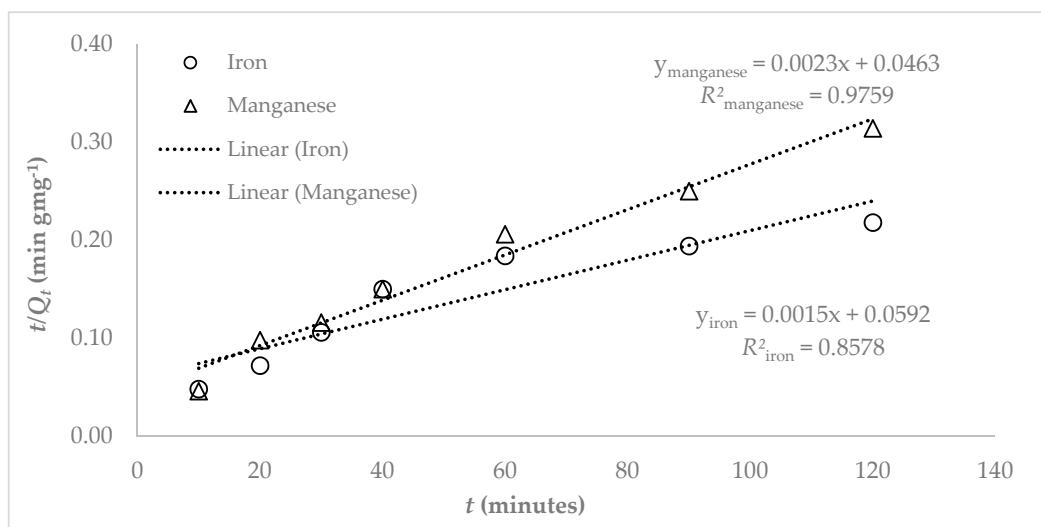


Figure 11. Pseudo second order kinetic model obtained for adsorption of iron and manganese on to zeolite Y. Initial Fe = 1.15 mg L⁻¹; Initial Mn = 1.61 mg L⁻¹; adsorbent dose = 2 g L⁻¹, T = 25 °C; water pH = 6.5.

Table 5. Kinetic parameters for iron and manganese onto zeolite Y.

	Pseudo First Order			Pseudo Second Order			Intra Particle Diffusion		Liquid Film	
	Q _e (mg g ⁻¹)	K ₁ (min)	R ²	K ₂ (g mg ⁻¹ min ⁻¹)	Q _e (mg g ⁻¹)	R ²	K _i (mg g ⁻¹ min ^{-½})	R ²	K _{fd}	R ²
Fe	0.221	0.026	0.963	3.8 × 10 ⁻⁵	0.235	0.858	0.009	0.967	5 × 10 ⁻⁵	0.602
Mn	0.282	0.043	0.911	1.1 × 10 ⁻⁴	0.267	0.976	0.012	0.949	7 × 10 ⁻⁵	0.756

When intra particle diffusion alone is the rate limiting step, then the plot of Q_t versus t^{1/2} passes through the origin. When film diffusion is also taking place then the intercept is C, which gives an idea of the thickness of the boundary layer.

The initial linear portion in the plot Fe and Mn adsorbed versus t^{1/2} (Figure 12) corresponds to the intra-particle diffusion process and the plateau to the equilibrium state. The values of K_i (=0.009 mg g⁻¹min^{-½}) for Fe(II) and (0.012 mg g⁻¹min^{-½}) for Mn(II) are equal to the slope of the intra-particle diffusion line. The fact that intra-particle diffusion curves did not cross the origin of the axes is indicative of the rapid adsorption of Fe(II) and Mn(II) onto the exterior surface of the adsorbent. However, the negative value of the intercept may be attributed to the fact that the surface of the zeolite did not slow down the rate of adsorption. Hence, the intra-particle diffusion was not the rate determining step in the adsorption process. Thus it was clear that from the intra particle diffusion plots shown in Figure 12 that the adsorption processes followed two steps: The first linear portion followed the boundary layer diffusion followed by another linear portion which represents the liquid film diffusion (Figure 13). This shows that the adsorption processes were not only by intra particle diffusion but the film diffusion also played a role in both the observed processes [35,36].

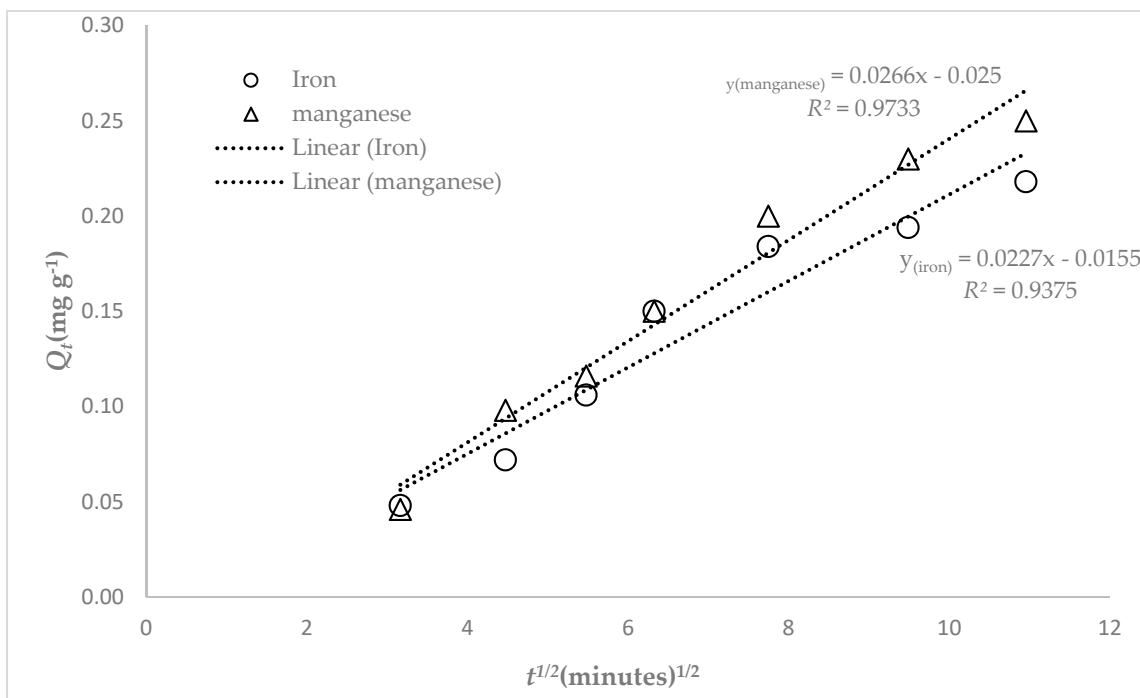


Figure 12. Intra-particle diffusion $t^{1/2}$ -dependence of iron and manganese adsorption capacity on to zeolite Y. Dashed lines indicate the linear fitting at intra-particle diffusion and equilibrium state regions. Initial Fe = 1.15 mg L⁻¹; Initial Mn = 1.61 mg L⁻¹; adsorbent dose = 2 g L⁻¹, T = 25 °C; water pH = 6.5.

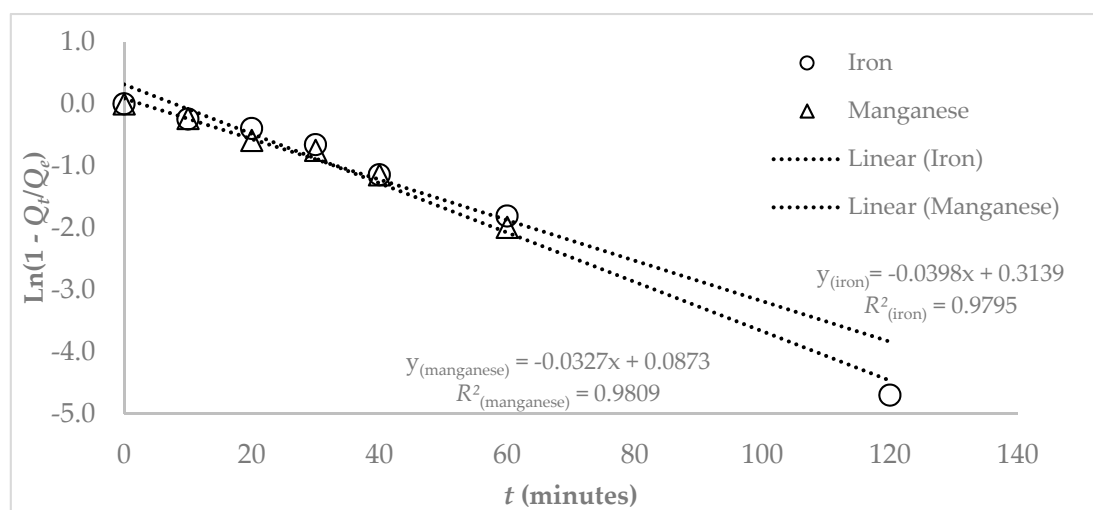
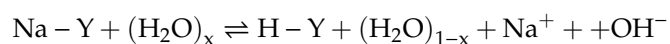


Figure 13. Linearized graph obtained for liquid film diffusion model for iron and manganese uptake on zeolite Y.

It is well established that the addition of zeolites to drinking water results in complex pH variations where ion exchange is accompanied by a variety of hydrolytic side reactions resulting in additional hydronium ion exchange as well as the precipitation of metal hydroxides [37–39]. As shown in Figure 14, the pH immediately increased upon an addition of the zeolite to reach a maximum after 5 min and then slowly to attain a fairly weak neutral (pH = 7.3–7.4). The immediate pH increase after the addition of Na-Y can be attributed to a hydrolysis of the zeolite [37,38].



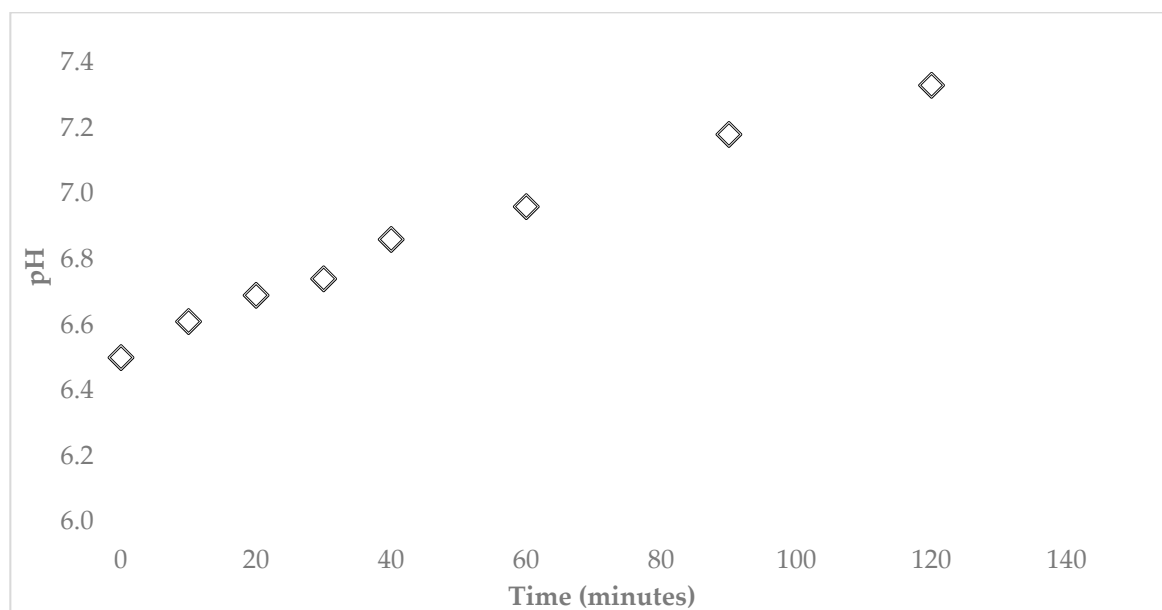


Figure 14. Results of pH of water during kinetic experiment of iron and manganese onto zeolite Y. Initial Fe = 1.15 mg L^{-1} ; Initial Mn = 1.61 mg L^{-1} ; adsorbent dose = 2 g L^{-1} , T = $25 \text{ }^\circ\text{C}$; water pH = 6.5.

The indigenous zeolitic sodium cations were partially exchanged by hydronium ions forming free hydroxide. The hydroxide formed is responsible for the pH increase of the solution. The addition of Na-Y to the water samples was also accompanied by an immediate increase in pH to a maximum value of 7.4 that then maintained to a constant value of 7.3 due to a partial dissolution of the zeolite in the alkaline solution accompanied by a consumption of hydroxide ions [32,40]. The increase in solution pH can be attributed to an uptake of the hydroxide ions originating from the hydrolysis of the zeolite [40,41]. Similar reaction sequences can be attributed to the removal of manganese ions from the water samples. However, since the maximum adsorption of Fe(II) and Mn(II) was achieved at a pH just below 7 (slightly acidic), it is safe to say that the removal of Fe(II) and Mn(II) were due to adsorption rather than to dissolution.

It has been reported that in general, manganese removal is higher than Mn for clinoptilolite, a natural zeolite [34,42]. Overall, Fe and Mn removal levels are 22–90% and 61–100% for clinoptilolite. These removal levels are comparable to the ones obtained by zeolite Y as shown in this work for the simultaneous iron and manganese removal from water samples. For instance, in a treatment of iron and manganese in simulated groundwater via ozone technology, at an ozone dose of 1.25 mg L^{-1} and an initial iron concentration of 2.6 mg L^{-1} and a manganese concentration of 1 mg L^{-1} , more than 90% of iron was removed, while just only 15% of manganese was eliminated at the same conditions. Increasing the ozone concentration to about 3 mg L^{-1} improved the removal of iron to more than 96% while about 83% of manganese was removed [43].

In another case, the biological removal of Fe (II) and Mn (II) from drilled well water in a biological treatment continuous flow unit in China, resulted in a 99% removal of Fe and 35–75% for Mn, under an initial concentration of 3–8 mg L^{-1} for Fe and 2 mg L^{-1} for Mn [35,38]. In this work both Fe(II) and Mn(II) were equally removed from the potable ground water.

5. Conclusions

Zeolite Y was successfully synthesized with bauxite and kaolin as source materials. Groundwater samples used in this study showed that iron and manganese were present at levels higher than the Ghana Standard Authority and WHO recommended levels. The removal of iron and manganese from potable water by zeolite Y was thoroughly investigated and found to remove both species without considerable alteration of the water profile. The zeolite retained its removal efficiency after two

successive instances of retrieval and re-use. The mechanism of adsorption was mainly pseudo-first order with intra particle diffusion occurring within the zeolite framework. The adsorption isotherm studies were more favorable to the Freundlich model. The zeolite Y can be said to present a high potential in its use as an adsorbent for heavy metal removal and for potable water treatment.

Author Contributions: Data curation, B.K.-A. and I.N.; formal analysis, B.K.-A., B.S.-N., E.V.-K. and C.W.; methodology, B.K.-A. and C.W.; validation, I.N.; writing—original draft, B.K.-A.; writing—review & editing, B.S.-N., E.V.-K., I.N. and C.W.

Funding: We are grateful to Third World Academy of Sciences (TWAS) (Grant # 16-471 RG/PHYS/AF/AC_G) and Grand Challenges Canada (Grant # RS-0148 -01)) for providing funds for the project.

Acknowledgments: The authors are grateful to Royal Society, UK and Grand Challenges Canada for their financial support.

Conflicts of Interest: The authors declare no conflict of interest.

Nomenclature

m	=	mass of zeolite Y
C_e	=	Equilibrium concentration
Q_e	=	Adsorption at equilibrium
Q_t	=	Adsorption at time t
$Q_{0.5}$	=	adsorption of iron at concentration of 0.5 mg L ⁻¹
$Q_{0.02}$	=	adsorption of manganese at concentration of 0.02 mg L ⁻¹
K_L	=	Langmuir constant parameter
K_F	=	Freundlich constant parameter
K_1	=	Pseudo-first order rate constant
K_2	=	Pseudo-second order rate constant
K_i	=	Intra-particle diffusion constant
K_d	=	diffusion constant

References

1. Barloková, D.; Ilavský, J. Removal of Iron and Manganese from Water Using Filtration by Natural Materials. *Pol. J. Environ. Stud.* **2010**, *19*, 1117–1122.
2. bin Jusoh, A.; Cheng, W.H.; Low, W.M.; Nora'aini, A.; Megat Mohd Noor, M.J. Study on the removal of iron and manganese in groundwater by granular activated carbon. *Desalination* **2005**, *182*, 347–353. [[CrossRef](#)]
3. Aziz, H.A.; Smith, P.G. Removal of manganese from water using crushed dolomite filtration technique. *Water Res.* **1996**, *30*, 489–492. [[CrossRef](#)]
4. Dorthel, J.; Jensk, B.S.; Thomash, C. Speciation of Dissolved Iron(II) and Manganese(II) in a Groundwater Pollution Plume. *Environ. Sci. Technol.* **1998**, *32*, 2657–2664.
5. AWWA; ASCE. *Water Treatment Plant Design*, 2nd ed.; McGraw-Hill Inc.: New York, NY, USA, 1990.
6. García-Mendieta, A.; Solache-Ríos, M.; Olguín, M.T. Evaluation of the sorption properties of a Mexican clinoptilolite-rich tuff for iron, manganese and iron–manganese systems. *Microporous Mesoporous Mater.* **2009**, *118*, 489–495. [[CrossRef](#)]
7. Inglezakisa, V.J.; Doulab, M.K.; Aggelatou, V.; Zorpas, A.A. Removal of iron and manganese from underground water by use of natural minerals in batch mode treatment. *Desalin. Water Treat.* **2010**, *18*, 341–346. [[CrossRef](#)]
8. WHO. *World Health Organization Guidelines*, 3rd ed.; WHO Press: Geneva, Switzerland, 2004; pp. 166–196.
9. Sarin, P.; Snoeyink, V.L.; Bebee, J.; Jim, K.K.; Beckett, M.A.; Clement, J.A. Iron release from corroded iron pipes in drinking water distribution systems: Effect of dissolved oxygen. *Water Res.* **2004**, *38*, 1259–1269. [[CrossRef](#)]
10. Aschner, A.; Erikson, K.M.; Hernández, E.H.; Tjalkens, R. Manganese and its Role in Parkinson's Disease: From Transport to Neuropathology. *Neuromol. Med.* **2009**, *11*, 252–266. [[CrossRef](#)]
11. WHO. *Guidelines for Drinking-Water Quality*, 2nd ed.; WHO Press: Geneva, Switzerland, 2011; pp. 1–21.

12. Ahmad, M. Iron and Manganese Removal from Groundwater: Geochemical Modeling of the Vyredox Method. Master's Thesis, University of Oslo, Oslo, Norway, 2012.
13. Awuah, J.B.; Dzade, N.Y.; Tia, R.; Adei, E.; Kwakye-Awuah, B.; Richard, C.; de Leeuw, N.H. A density functional theory study of arsenic immobilization by the Al(III)-modified zeolite clinoptilolite. *Phys. Chem. Chem. Phys.* **2016**, *18*, 11297–11305. [[CrossRef](#)]
14. Erdem, E.; Karapinar, N.; Donat, R. The removal of heavy metal cations by natural zeolites. *J. Coll. Interface Sci.* **2004**, *280*, 309–314. [[CrossRef](#)]
15. Singer, P.A.; Salamanca-Buentell, F.; Daar, A. Harnessing Nanotechnology to Improve Global Equity. *Issues Sci. Technol.* **2005**, *21*, 57–64.
16. Lin, L.; Lei, Z.; Wang, L.; Liu, X.; Zhang, Y.; Wan, C.; Lee, D.; Tay, J.H. Adsorption mechanisms of high-levels of ammonium onto natural and NaCl-modified zeolites. *Sep. Purif. Technol.* **2013**, *103*, 15–20. [[CrossRef](#)]
17. Tsitsishvili, G.V.; Andronikashvili, T.G.; Kirov, G.N.; Filizova, L.D. *Natural Zeolite*; Ellis Horwood: New York, NY, USA, 1992.
18. Yusof, A.M.; Malek, N.A.N.N. Removal of Cr (VI) and as (V) from aqueous solutions by HDTMA-modified zeolite Y. *J. Hazard. Mater.* **2009**, *162*, 1019–1024. [[CrossRef](#)] [[PubMed](#)]
19. Li, Z.; Beachner, R.; McManama, Z.; Hanlie, H. Sorption of arsenic by surfactant-modified zeolite and kaolinite. *Micropor Mesopor Mater.* **2007**, *105*, 291–297. [[CrossRef](#)]
20. Payne, K.; Abdel-Fattah, T. Adsorption of Arsenate and Arsenite by Iron-Treated Activated Carbon and Zeolites: Effects of pH, Temperature, and Ionic Strength. *J. Environ. Sci. Health Part A* **2005**, *40*, 723–749. [[CrossRef](#)]
21. Ahmed, S.; Chughtai, S.; Keane, M.A. The removal of cadmium and lead from aqueous solution by ion exchange with Na-Y zeolite. *Sep. Purif. Technol.* **1998**, *13*, 57–64. [[CrossRef](#)]
22. Keane, M.A. Microporous Materials. Role of the alkali metal co-cation in the ion exchange of Y zeolites III. Equilibrium properties of the Ni/Cu/Na-Y and Ni/Cu/K-Y zeolite systems. *Microporous Mater.* **1995**, *4*, 359–368. [[CrossRef](#)]
23. Shevade, S.; Ford, R.G. Use of synthetic zeolites for arsenate removal from pollutant water. *Water Res.* **2004**, *38*, 3197–3204. [[CrossRef](#)] [[PubMed](#)]
24. Kwakye-Awuah, B.; Williams, C.; Kenward, M.A.; Radecka, I. Antimicrobial action and efficiency of silver-loaded zeolite X. *J. Appl. Microbiol.* **2008**, *104*, 1516–1524. [[CrossRef](#)] [[PubMed](#)]
25. Kwakye-Awuah, B.; Labik, L.K.; Nkrumah, I.; Williams, C. Removal of ammonium ion by laboratory-synthesized zeolite LTA adsorption from waters samples affected by mining activities in Ghana. *J. Water Health* **2014**, *12*, 151–160. [[CrossRef](#)] [[PubMed](#)]
26. Kim, J.S.; Zhang, L.; Keane, M.A. Removal of iron from aqueous solutions by ion exchange with NA-Y zeolite. *Sep. Sci. Technol.* **2013**, *36*, 1509–1525. [[CrossRef](#)]
27. Mozgawa, W. The influence of some heavy metals cations on the FTIR spectra of zeolites. *J. Mol. Struct.* **2000**, *555*, 299–304. [[CrossRef](#)]
28. Kwakye-Awuah, B.; Von-Kiti, E.; Nkrumah, I.; Ikyereve, R.E.; Williams, C. Parametric, Equilibrium, and Kinetic Study of the Removal of Salt Ions from Ghanaian Seawater by Adsorption onto Zeolite X. *Desalin. Water Treat.* **2016**, *57*, 21654–21663. [[CrossRef](#)]
29. Coutinho, D.; Balkus, J.K., Jr. Preparation and characterization of zeolite X membranes via pulsed-laser deposition. *Microporous Mesoporous Mater.* **2002**, *52*, 79–91. [[CrossRef](#)]
30. Saha, U.K.; Taniguuchi, S.; Sakurai, K. Simultaneous sorption of cadmium, zinc, and lead on hydroxyaluminum- and hydroxyaluminosilicate-montmorillonite complexes. *Soil Sci. Soc. Am. J.* **2002**, *66*, 117–128. [[CrossRef](#)]
31. Fu, G.; Allen, H.E.; Cowan, C.E. Adsorption of cadmium and copper by manganese oxide. *Soil Sci.* **1991**, *152*, 72–81. [[CrossRef](#)]
32. Gouzinis, A.; Kosmidis, N.; Vayenas, D.V.; Lyberatos, G. Removal of Mn and Simultaneous Removal of NH₃, Fe, and Mn from Potable Water Using a Trickling Filter. *Water Res.* **1998**, *32*, 2442–2450. [[CrossRef](#)]
33. Farrag, A.H.A.; Moghny, T.A.; Gad Mohamed, A.M.G.; Saleem, S.S.; Fathy, M. Abu Zenima synthetic zeolite for removing iron and manganese from Assiut governorate groundwater, Egypt. *Appl. Water Sci.* **2017**, *7*, 3087–3094. [[CrossRef](#)]

34. Yavuz, O.; Altunkaynak, Y.; Guzel, F. Equilibrium and Kinetics Study for Adsorption of 2,4-Dinitrophenol from Aqueous Solutions by Using Cucumis Sativus Peels and Kidney Bean Shells as New Low-cost Adsorbents. *Water Res.* **2003**, *37*, 948. [[CrossRef](#)]
35. Wei-Wei, B.; Hai-Feng, Z.; Shu-Cai, G.; Xue-Chun, X.; Gui-Juan, J.; Ke-Yan, Z. Adsorption of Heavy Metal Ions from Aqueous Solutions by Zeolite Based on Oil Shale Ash: Kinetic and Equilibrium Studies. *Chem. Res. Chin. Univ.* **2013**, *29*, 126–131.
36. Araby, R.E.; Hawash, S.; Diwani, G.E. Treatment of iron and manganese in simulated groundwater via ozone technology. *Desalination* **2009**, *249*, 1345–1349. [[CrossRef](#)]
37. Novembre, D.; Sabatino, B.D.; Gimeno, D.; Garcia-Valles, M.; Martinez-Manent, S. Synthesis of Na-X zeolites from tripolaceous deposits (Crotone, Italy) and volcanic zeolitised rocks (Vico volcano, Italy). *Microporous Mesoporous Mater.* **2004**, *75*, 1–11. [[CrossRef](#)]
38. Han, R.; Zou, W.; Zhang, Z.; Shi, J.; Yang, J. Removal of copper(II) and lead(II) from aqueous solution by manganese oxide coated sand I. Characterization and kinetic study. *J. Hazard. Mater. B* **2006**, *137*, 384–395. [[CrossRef](#)] [[PubMed](#)]
39. Wark, M.; Lutz, W.; Schulz-Ekloff, G.; Dyer, A. Quantitative monitoring of side products during high loading of zeolites by heavy metals via pH measurements. *Zeolites* **1993**, *13*, 658. [[CrossRef](#)]
40. Silvio, R.T.; Rubio, T.J. Removal of Mn²⁺ from aqueous solution by manganese oxide coated zeolite. *Miner. Eng.* **2010**, *23*, 1131–1138.
41. Sefa-Ntiri, B.; Kwakye-Awuah, B.; Mensah-Amoah, P.; Williams, C. Removal of Pb²⁺ and Fe²⁺ from Water Samples in Ghana by Synthetic Zeolites as Measured by Atomic Absorption Spectroscopy and Light Transmission Experiments. *Int. J. Sci. Res.* **2015**, *4*, 220–227.
42. Qin, S.; Ma, F.; Huang, P. Membrane Processes: Development, Monitoring and Modelling from the Nano to the Macro Scale. *J. Desalin.* **2009**, *245*, 183–193. [[CrossRef](#)]
43. Vasanth, K.K.; Ramamurthi, V.S.S. Modeling the mechanism involved during the sorption of methylene blue onto fly ash. *J. Colloid Interface Sci.* **2005**, *284*, 14–21.



© 2019 by the authors. Licensee MDPI, Basel, Switzerland. This article is an open access article distributed under the terms and conditions of the Creative Commons Attribution (CC BY) license (<http://creativecommons.org/licenses/by/4.0/>).